PAPER • OPEN ACCESS

Design and characterisation of multi-mode interference reflector lasers for integrated photonics

To cite this article: F T Albeladi *et al* 2023 *J. Phys. D: Appl. Phys.* **56** 384001

View the article online for updates and enhancements.

Design and characterisation of multi-mode interference reflector lasers for integrated photonics

F T Albeladi[1,2,*] ⓘ, **S Gillgrass**[1] ⓘ, **J Nabialek**[1], **P Mishra**[1], **R Forrest**[1], **T R Albiladi**[1,3], **C P Allford**[1] ⓘ, **H Deng**[4], **M Tang**[4] ⓘ, **H-Y Liu**[4] ⓘ, **S Shutts**[1] **and P M Smowton**[1,*]

[1] School of Physics and Astronomy, Cardiff University, The Parade, Cardiff CF24 3AA, United Kingdom
[2] Physics Department, Faculty of Science, University of Jeddah, Jeddah 21589, Saudi Arabia
[3] Physics and Astronomy Department, Faculty of Science, King Saud University, Riyadh 11451, Saudi Arabia
[4] Department of Electronic and Electrical Engineering, University College London, Torrington Place, London, United Kingdom

E-mail: albeladiFT@cardiff.ac.uk and smowtonpm@cardiff.ac.uk

CrossMark

Abstract

InAs quantum dot ridge waveguide lasers comprising single-port multi-mode-interference-reflectors (MMIR) and single-cleaved reflectors are designed, fabricated, and characterised, to demonstrate capability for optoelectronic-integrated-circuits. Simulations of an MMIR show high values of fundamental mode reflectivity ($> 80\%$) and good selectivity against higher order modes. Deep-etched MMIR lasers fabricated with 0.5 mm long cavities have a threshold current of 24 mA, compared to 75 mA for standard Fabry–Perot cleaved–cleaved FP-RWG lasers of the same length, both at 25 °C, and 56 mA compared to 102 mA at 55 °C. MMIR lasers exhibit stable ground state operation up to 50 °C and show promise as small footprint sources for integrated photonics.

Keywords: QDs, photonics, integration, laser reflectors

(Some figures may appear in colour only in the online journal)

1. Introduction

Much work is currently focussed on developing platforms for the integration of light sources and other photonic elements and ultimately, for the co-integration of photonic and electronic functions. Probably the most elegant approach involves direct epitaxial growth of III–V semiconductors on silicon and the best performing lasers, in terms of current density and reliability, use 1.3 μm-emitting InAs quantum dots (QDs) [1–4]. However, this good performance has only been achieved with low optical loss per unit length structures, often with very long cavity lengths or coated facets. It is also well understood that the optical gain achieved from the QD materials is relatively low. Consequently, any increase in mirror loss that occurs due to poorer quality reflectors is particularly detrimental. This poses a difficulty for III–V QD lasers directly grown on silicon as part of an integrated circuit, where a small footprint is required and where coated facets can be difficult to implement.

Mirror losses play a crucial role in the performance of a laser. The quality of the mirrors used in a laser cavity determines the threshold current, including its temperature

---

* Authors to whom any correspondence should be addressed.

dependence, the amount of light that is lost from the cavity and the overall efficiency of the laser. Reducing the mirror loss is important in QD lasers because of the relatively low maximum gain and has produced the lowest threshold current density of any type of laser [5] and can improve the reliability of QD lasers [6].

Several different reflector types have been suggested for photonic integrated circuits and must be of high quality for integrated lasers. These include cleaved or etched facets, distributed feedback (DFB) elements, deep-etched distributed Bragg reflectors (DBRs) and loop-mirrors; each having pros and cons. Cleaved facets can only be used at the edge of the integrated circuit and etched facets are generally of slightly lower reflectivity due to imperfect side wall angle and roughness [7] that can be introduced during the etching process. DFBs [8], which can be of the sidewall or lateral type [9] to avoid localised or multiple regrowth steps, and photonic crystal or deep-etched DBRs, can be effective, the latter with only a few grating periods, to achieve high reflectivity. However, these generally require e-beam lithography for the feature size required, increasing cost and manufacturing time. Furthermore, the combination of process steps required for these fine-featured, deep etched structures, with the fabrication required for other process steps increases fabrication complexity considerably if the performance of all components is to be maintained. While first-order gratings require e-beam lithography for most wavelengths of interest for integrated photonics, higher order gratings ($N > 10$) have been suggested for standalone lasers [10–12]. DBR periods above approximately 2 μm can be achieved using photolithography, which is already multiple order gratings for an operating wavelength, $\lambda \cong 1.3$ μm. An increase of the DBR period gives rise to high diffraction orders emitting outside the plane of the heterostructure waveguide, increasing parasitic optical output losses [13]. Consequently, increasing DBR period adds a loss penalty on the laser performance, whereby the threshold current is increased and the laser efficiency reduced, when compared with Fabry–Perot lasers of the same cavity length [14]. Loop-mirrors can be highly reflective but require a relatively large footprint on chip, on the scale of $\approx$mm, $\cong$ mm in addition to the fabrication requirement of low side-wall roughness to minimise the bend loss [15, 16].

Here we focus on the multi-mode-interference reflector (MMIR) [17, 18], which offers advantages with regard to reflectivity and footprint, and demonstrate it can be effective when creating InAs QD semiconductor lasers.

The principle of a single port MMIR is shown in figure 1, and it should be possible to create this type of device with low loss and in a format that is relatively insensitive to wavelength and polarization [17, 18]. An MMI can also be an important element in the loop mirror, but here it is used with two superimposed 45° mirrors forming the MMIR, whereby total internal reflection occurs, and light is imaged back on the input waveguide. MMIs are established components [19] and are widely used in photonic integrated circuits, and their widespread and successful use suggests they offer relatively stable
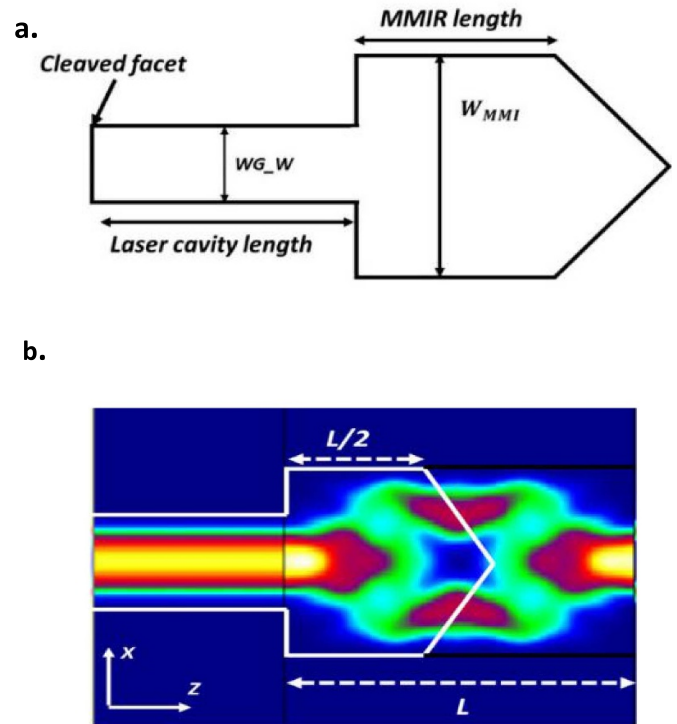

Figure 1. (a) Schema of the MMIR laser used here—not to scale. The length of the MMIR is always less than 10% of the total length. (b) Operation principle: field distributions simulation of a 1 × 2 MMI with the position of two superimposed angled facets marked.

performance to typical variations arising in the fabrication process [20]. Adding an angled end mirror does not add significant complexity to the fabrication. One-port MMIRs provide higher reflectivity and lower loss [21, 22], which translates to higher efficiency and a simpler design, compared to two-port MIRs, making them a versatile choice for a range of applications where a simple reflector is required. We test the single port MMIR in a laser cavity.

In this work, we describe the modelling and design, fabrication, and characterization of MMIR lasers based on InAs QDs grown on GaAs. Here, both the laser active region and the reflector components are made from the same material, as a means to qualify the performance of these reflectors for use with QD material.

2. Device design

Unlike a simple MMI, the propagation inside the MMIR mirror element is multi-directional. As a result, the simulation approach has to be changed from that conventionally used for an MMI. With the assumption that the mirrors are perfect, then the simulation can be carried out with a combination of bidirectional and unidirectional methods. Here modelling of the MMIR is carried out using the commercially available Photon Design software. The first part of the MMIR is
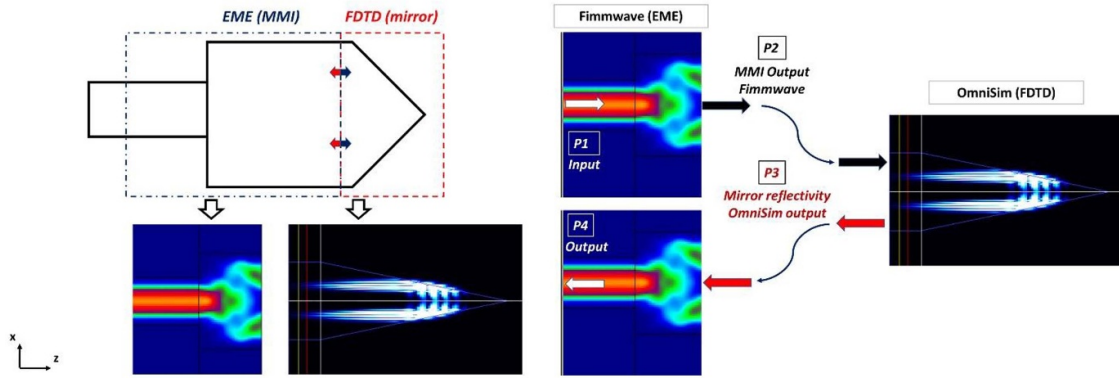
Figure 2. The MMIR is divided into two parts: an eigenmode expansion (EME) method is used to simulate the first section. The field is stored and launched into a finite difference time domain (FDTD) simulation. The output field of the FDTD is then launched back into the EME simulation. The overlaps with the access waveguide modes are then calculated to obtain device reflection and transmission coefficients.

simulated using an eigenmode expansion (EME) method. The field is then stored and launched into a finite difference time domain (FDTD) model as represented in figure 2. The output is subsequently launched back into the EME model. The overlaps with the access waveguide modes are then calculated to obtain device reflection and transmission coefficients.

The MMIR reflectivity, R_{total}, is determined from the simulation using the following expression:

$$R_{\text{total}} = \frac{P_2}{P_1} \times \frac{P_3}{P_2} \times \frac{P_4}{P_3} \qquad (1)$$

where P_1 and P_2 are the input and output power from the MMI propagating into the mirror section; P_3 is the reflected power at the 45°mirror, and P_4 is the output power transferred from the MMI back into the RWG of the laser. Figure 2 illustrates the mode profile within the sections of the MMIR. The EME solver (Fimmwave software) was used to determine the optimum length of the MMI in order to maximise P_1, P_2, P_4 of the MMI while an FDTD solver (OmniSim software) was used to optimise the reflectivity (P_3) as a function of mirror angle and wavelength. By dividing the MMIR into two parts and selectively applying either EME or FDTD, the simulation can be optimised in terms of speed and accuracy, so both the accuracy and the speed of EME and the multi-directionality of FDTD can be utilised.

This approach was used to optimise an InAs QD laser with a deep etched waveguide. The simulated 1×2-port MMI was designed for a layer stack with an effective index of 3.3 as shown in figure 3(a). The MMI length is optimised at 46 μm as shown in figure 3(b) to create a 50/50 light distribution at the output of the MMI. The MMIR mirror tip (see figure 2) should ideally be placed at a null in the intensity in the *x*-direction such that the reflectors are at the calculated peak output intensity of the MMI in the *z*-direction [19]. Due to lithographical effects, the mirror's tip is often rounded (see later). As a result, any light projected there will not be properly reflected, resulting in a loss penalty.

The mirror reflectivity is simulated using FDTD (OmniSim software) as a function of mirror angle and wavelength, as shown in figures 4(a) and (b). Figure 4(b) shows the intensity reflectivity (R_0) resulting from the fundamental TE_{00} mode, which is calculated from the overlap of the total power through the simulation sensor with the fundamental TE_{00} mode of the waveguide.

For the MMIR reflector with a 46 μm MMI length and 45-degree mirror angle, the intensity reflectivity obtained for the fundamental TE_{00} mode can be higher than 80% and this is obtained over a wide wavelength range between 1.2–1.35 μm. The MMIR has maximum reflectivity at 45 degrees at a desired operating wavelength of 1.31 μm for the fundamental mode power.

The MMI is designed and optimised for TE_{00}, based on the symmetric interference mechanism [17, 19], to combine the reflected light from both mirror sides. The MMI interference pattern produced by the input field (power, P_1) from the fundamental TE mode (TE_{00}) is illustrated in figure 5(a) and the first and second order TE mode (TE_{01}) and (TE_{02}) in figures 5(b) and (c). When a TE_{00} mode, enters the input port of the 1×2 MMI, its power will be equally split and constructive interference occurs at the centre of the two MMI outputs [16] as shown in figure 5(a). Figure 5(d) illustrates the power reflectance of the MMIR TE_{00}, TE_{01} and TE_{02} modes (*y*-axis) for inputs in each of these modes (*x*-axis). For input in TE_{00} 80% is reflected in TE_{00}, a few percent in TE_{02} and 0% reflected in TE_{01}.

The MMI performs very efficiently as a power splitter, and simulation shows that the combined power transfer efficiency to the two ports of the MMI is approximately 99% for TE_{00} (twice the power per port of figure 3(b)), indicating that the output field from the MMI will be two replicated TE_{00} modes which are subsequently reflected back to the input MMI when the reflectors are inserted. As shown in figure 5(b), the asymmetric-order modes TE_{01} interfere destructively at the centre, whereas the symmetric-order modes TE_{02} (see figure 5(c)) interfere constructively at the centre. In figure 5(d), simulations show that outgoing fields from the MMIR are combined by the MMI coupler, with resulting reflectivity of 83% for TE_{00} and 38% for TE_{02} (symmetric mode) when the
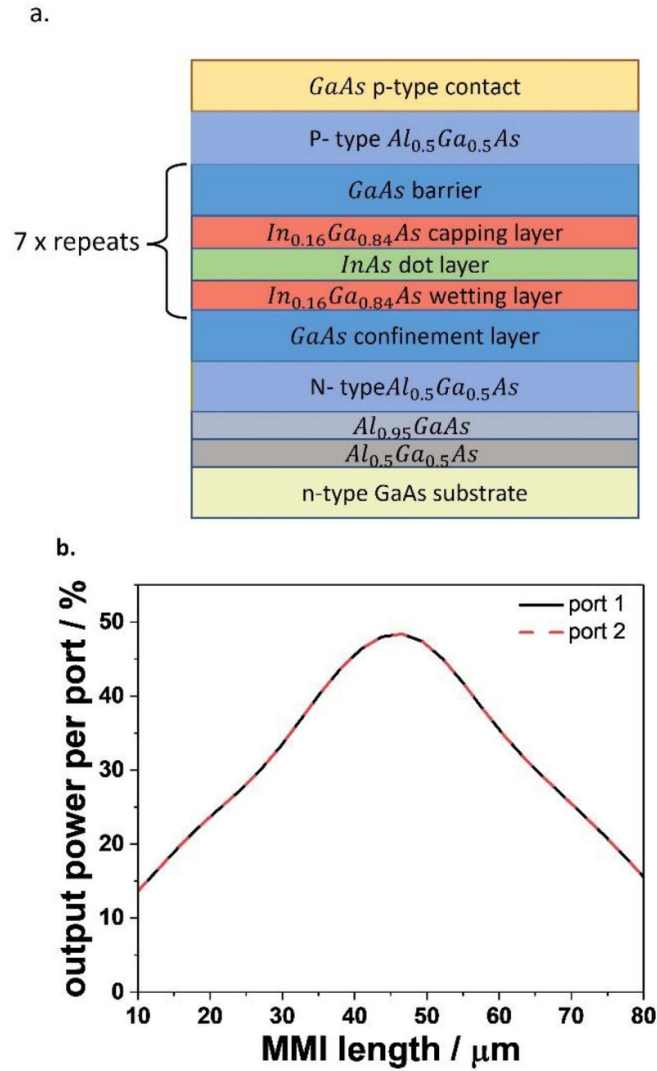
a.

b.

Figure 3. (a) 1.31 μm InAs QD epi-structure of grown and simulated samples with seven DWELL layers. (b) Simulated 1×2 MMI output power per MMI port as a function of MMI length by Fimmwave (EME method). Note: data for port 1 and port 2 overlay each other.

input mode (P_1) is the TE$_{00}$ and TE$_{02}$ respectively. However, the reflectivity of the TE$_{01}$ (asymmetric mode) is less than 2%. It is noted that the outgoing power (P_4) from MMIR contains mostly the TE$_{00}$ mode, which is a symmetric-order mode. The missing TE$_{01}$ mode will be reflected in the comparison of the laser spectra for the MMIR and the standard Fabry–Perot with two-cleaved facet ridge waveguides (FP-RWG) lasers (see later).

In summary, the MMIR can be used to filter out the asymmetric order modes created in an input waveguide and so the single mode ridge part of the laser can be made slightly wider (and thus more tolerant to fabrication uncertainty) than a standalone RWG laser structure.

3. Device fabrication and testing

To investigate actual performance, we fabricated 3 μm wide InGaAs–InAs QD MMIR RWG lasers, with 6 μm wide, 46 μm long MMI section terminated with two, 45-degree angled,

deep-etched mirrors (layout figure 1(a)). To avoid ambiguity the reflectors were demonstrated here in lasers where the other mirror is a cleaved facet and will be used with simple etched facets or other reflector elements in integrated circuits. Both the MMIR and RWG were defined using a single photolithography step, and the pattern transferred by way of a Cl$_2$-based inductively coupled plasma etch. The devices were etched through the entirety of the epitaxial layers, to the substrate. Spin-coating of benzocyclobutane (BCB) and subsequent back-etching provided planarisation to the height of the MMIR and RWG. A Ti/Au stack was deposited, and patterned via a liftoff process, for the *p*-Ohmic contact, followed by standard AuGe/Ni/Au blanket deposition for the global *n*-metal contact. Prior to the *n*-contact deposition, the sample was thinned to approximately 100 μm, to allow for a high-quality cleaved facet of the RWG. Following fabrication, devices were cleaved into either 0.5 mm, 1 mm, 2 mm, or 3 mm lengths. An example of a fabricated device is pictured in figure 6(a), with a plan view image taken using an optical microscope, showing a section of the 3 μm wide RWG covered
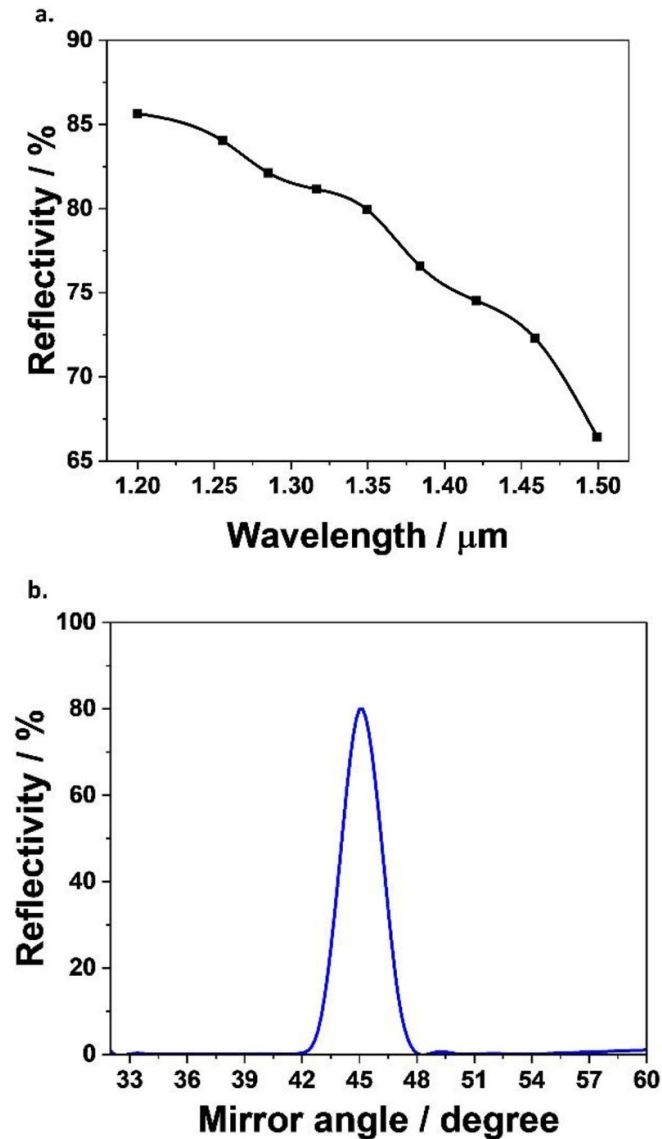
Figure 4. (a) The MMIR reflectivity as a function of wavelength at mirror angle 45°. (b) MMIR reflectivity as function of mirror angle at 1.31 μm wavelength.

in p-metal, and the relatively short and slightly wider MMIR section. A separate image of the etched-angled end section of the MMIR is shown in figure 6(b), taken using a field-emission scanning electron microscope (FE-SEM). Characterization was carried out to compare the performance of these MMIR lasers with simple Fabry–Perot RWG lasers with two cleaved-facets (FP-RWG) of the same ridge width and fabricated in an identical manner. The cleaved facet reflectivity is estimated theoretically from the Fresnel equation for normal incidence using the effective index of the mode and for the 3 μm RWG width, this was calculated to be 29%.

Figure 7 shows peak power and efficiency as a function of current for the one port MMIR-cleaved facet and two-cleaved-facet FP-RWG lasers with pulsed sources operated on 0.5% duty cycle. Figure 7(a) shows that 0.5 mm and 1 mm long MMIR lasers have significantly lower threshold current and higher slope efficiency than FP-RWG lasers of the same

length. The threshold current of 1 mm long MMIR laser is 18 mA compared to 70 mA for the FP-RWG laser and the single facet external differential efficiency is also significantly increased for the 0.5 mm and 1 mm long MMIR lasers compared to the FP-RWG lasers. The 1 mm MMIR lasers also exhibit a less temperature-sensitive threshold current, albeit over the limited temperature range measured here, compared with FP-RWG lasers for the same cavity length (see figure 7(b)). The improved threshold current density and slope efficiency of the MMIR laser is too large to be caused by the very small difference in cavity length and is consistent with the much lower mirror loss of the MMIR reflector. This has a dramatic effect on threshold current and temperature dependence of threshold current because of the very saturated nature of the QD gain-current density curve (e.g. [23]).

The threshold current density for different cavity lengths is plotted in figure 8 as a function of temperature and shows
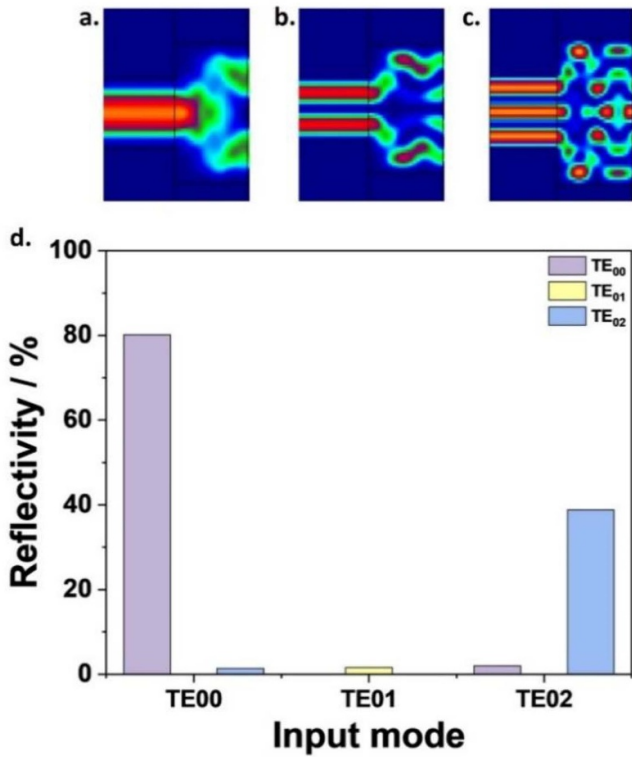
Figure 5. Electric field intensity in the MMI coupler showing the wave propagation for (a) fundamental mode TE_{00}, (b) second order straight mode TE_{01} as an example of asymmetric -order modes, and (c) third-order straight mode TE_{02} as an example of symmetric-order modes. (d) The MMIR reflectivity for these different order input modes, the purple column shows the ratio of TE_{00} from the total MMIR reflectivity of these different input order modes.
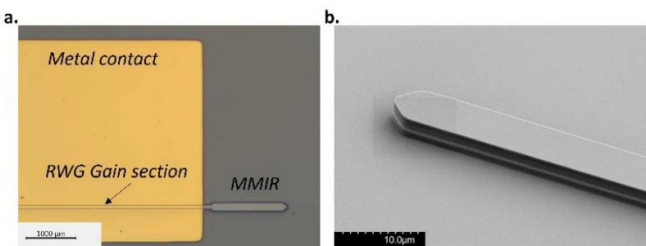

Figure 6. (a) Optical microscopic image of InAs QDs based MMIR laser (left), (b) FE-SEM micrograph of zoomed area of MMIR (right).

Figure 7. (a) Pulsed *P–I* curves for MMIR (solid) and FP-RWG (dashed) 0.5 mm (black) and 1 mm (red) cavity length lasers 25 °C, (b) *P–I* for MMIR (solid lines) and FP-RWG (dashed lines) laser for 1 mm cavity length as function of temperature.

improved performance for all lengths and temperatures for the MMIR lasers, demonstrating the effectiveness of the reduced mirror loss. Notably, the MMIR laser with 0.5 mm cavity length achieves a lower current density than the FP-RWG laser with 1 mm cavity length. The slope efficiency and threshold current data are consistent with a much higher mirror reflectivity for the MMIR mirror than the corresponding cleaved mirror for the FP-RWG lasers. Figure 9 shows that MMIR lasers operate on the QD ground state (at wavelengths around 1300 nm) down to 0.5 mm cavity length. This is the case up to temperatures of 50 °C, compared to the FP-RWG lasers where the 0.5 mm long laser operates on the excited state (wavelengths
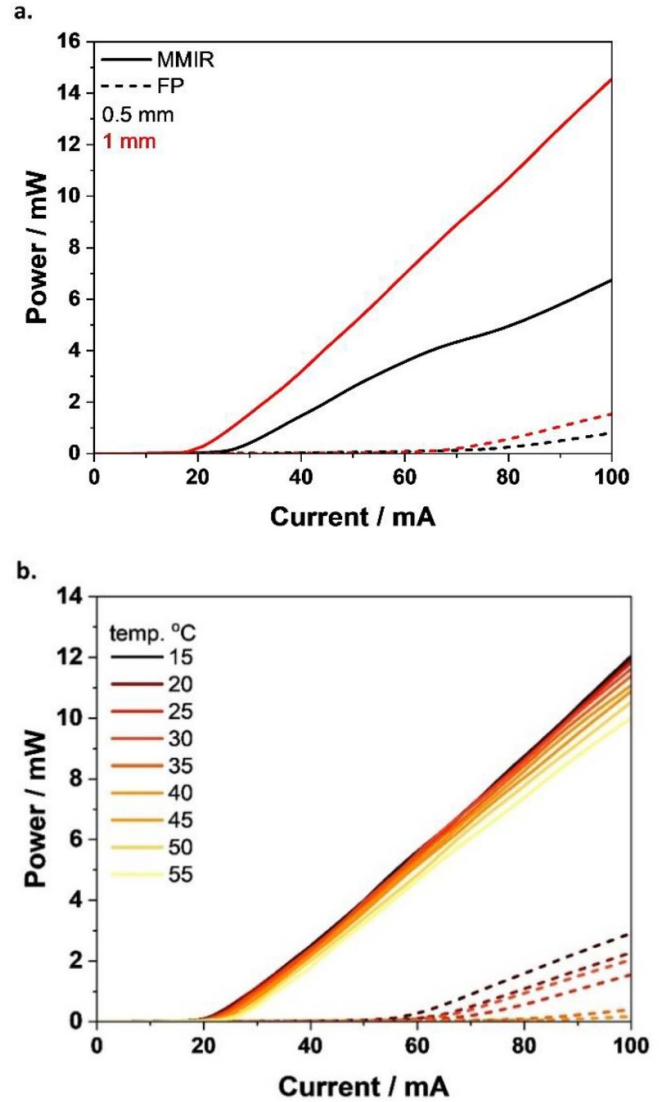
around 1200 nm) even at 15 °C. Again such results are consistent with a reduced mirror loss and gain requirement meaning sufficient gain can be obtained from the ground state for the MMIR lasers even at higher temperatures where the increased thermal distribution of carriers reduces the available gain [24].

Figure 10 shows the wavelength spectra at 20 and 45 °C for MMIR and FP-RWG lasers with 0.5 mm cavity length, in (a) and (b) respectively, and FP-RWG with 1 mm cavity length in (c). The spectra exhibit multiple lateral and longitudinal modes. The MMIR 0.5 mm lasing spectrum covers a smaller wavelength range and has a larger mode spacing compared with the FP-RWG laser spectrum with cavity lengths 0.5 mm and 1 mm. The larger spacing reflects the low MMIR reflectivity for the asymmetric lateral mode as presented in figure 5 meaning that the MMIR acts as a mode filter removing the asymmetric lateral modes. The narrower spectrum of the MMIR lasers reflects the fact that the lower mirror loss leads to
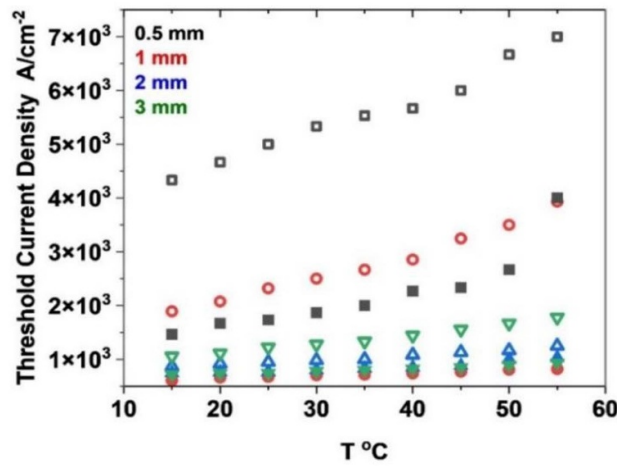
Figure 8. Threshold current density for MMIR (solid symbols) and FP-RWG (open symbols) lasers for 0.5, 1, 2 and 3 mm cavity length as function of temperature.
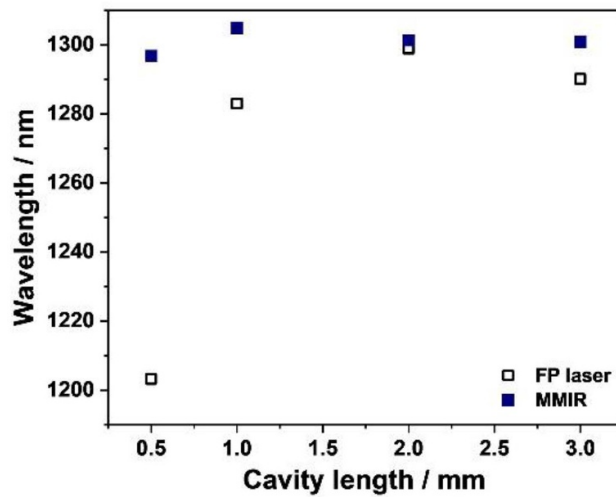

Figure 9. Peak lasing wavelength at $1.1 \times I_{th}$ for MMIR (solid squares) and FP-RWG lasers (open squares) for 0.5, 1, 2 and 3 mm cavity length at 25 °C.
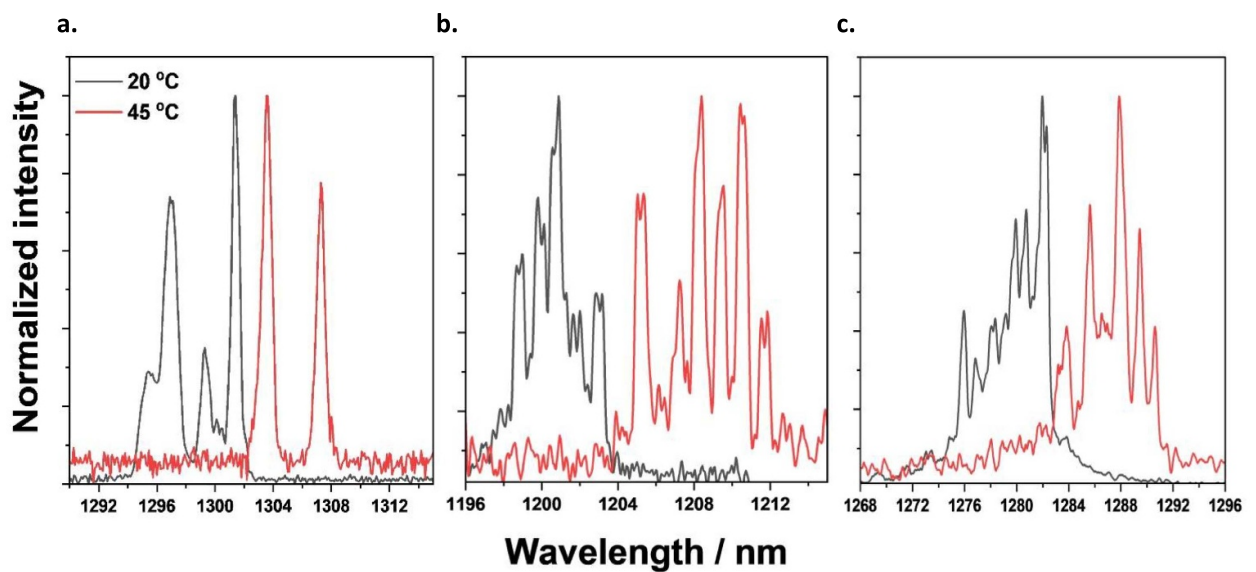

Figure 10. Emission spectra at 20 and 45 °C for (a). MMIR 0.5 mm cavity length, (b) and (c). FP-RWG laser with 0.5- and 1-mm cavity length respectively, at $1.1 \times I_{th}$. Wavelengths around 1300 nm correspond to the QD ground state whereas 1205 nm corresponds to the excited state.

a lower gain requirement and a lower threshold carrier density and thus narrower spectrum [24].

4. Summary

High reflectivity on-chip reflectors, fabricated with a single etch step, were used to improve the performance of InAs QD lasers. This demonstrates their suitability as reflectors and for use as one of the mirrors in lasers for integrated photonics. The reflectors formed from an MMIR have a small footprint, can be flexibly positioned and oriented anywhere in the circuit. The results shows that the lasers with one MMIR and one cleaved facet have lower threshold current, which is also less temperature dependant, compared to FP-RWG lasers with two cleaved facets and of equivalent length. The higher optical slope efficiency measured from the cleaved end of the MMIR laser indicates a mirror reflectivity higher than 80% compared to 30% for as laser with both facets cleaved. The laser incorporating a single port MMIR outperformed simple—FP-RWG devices with operation on the QD ground state up to 50 °C.

Data availability statement

The data that support the findings of this study are openly available at the following URL/DOI: https://doi.org/10.17035/d.2023.0246029130.

Acknowledgments

ORCID iDs

F T Albeladi ⬤ https://orcid.org/0000-0002-6587-7255
S Gillgrass ⬤ https://orcid.org/0000-0003-2611-9168
C P Allford ⬤ https://orcid.org/0000-0002-3798-9014
M Tang ⬤ https://orcid.org/0000-0001-6626-3389
H-Y Liu ⬤ https://orcid.org/0000-0002-7654-8553

References

[1] Chen S *et al* 2016 Electrically pumped continuous-wave III-V quantum dot lasers on silicon *Nat. Photon.* **10** 307–11
[2] Shang C, Wan Y, Selvidge J, Hughes E, Herrick R, Mukherjee K, Duan J, Grillot F, Chow W W and Bowers J E 2021 Perspectives on advances in quantum dot lasers and integration with Si photonic integrated circuits *ACS Photon.* **8** 2555–66
[3] Zhang Z, Shang C, Norman J C, Koscica R, Feng K and Bowers J E 2022 Monolithic passive−active integration of epitaxially grown quantum dot lasers on silicon *Phys. Status Solidi* **219** 2100522
[4] Shang C, Hughes E, Wan Y, Dumont M, Koscica R, Selvidge J, Herrick R, Gossard A C, Mukherjee K and Bowers J E 2021 High-temperature reliable quantum-dot lasers on Si with misfit and threading dislocation filters *Optica* **8** 749
[5] Deppe D G, Shavritranuruk K, Ozgur G, Chen H and Freisem S 2009 Quantum dot laser diode with low threshold and low internal loss *Electron. Lett.* **45** 54–56
[6] Shutts S, Allford C P, Spinnler C, Li Z, Sobiesierski A, Tang M, Liu H and Smowton P M 2019 Degradation of III-V quantum dot lasers grown directly on silicon substrates *IEEE J. Sel. Top. Quantum Electron.* **25** 1–6
[7] Yao R, Lee C-S and Guo W 2016 InAs quantum dot lasers with dry etched facet by Br-ion beam-assisted etching *IEEE Photonics Technol. Lett.* **28** 1905–7
[8] Wan Y *et al* 2020 1.3 *μ*m quantum dot-distributed feedback lasers directly grown on (001) Si *Laser Photon. Rev.* **14** 2000037
[9] Xu C, Chen S, Jin Y, Chen W and Zhu N 2022 A novel grating coupling coefficient extraction method for DFB laser diodes based on side mode spacing *IEEE Photon. J.* **14** 1–5
[10] Zolotarev V V, Leshko A Y, Pikhtin N A, Lyutetskiy A V, Slipchenko S O, Bakhvalov K V, Lubyanskiy Y V, Rastegaeva M G E and Tarasov I Y S 2014 Spectral characteristics of multimode semiconductor lasers with a high-order surface diffraction grating *Quantum Electron.* **44** 907
[11] Decker J, Crump P, Fricke J, Maassdorf A, Erbert G and Tränkle G 2014 Narrow stripe broad area lasers with high order distributed feedback surface gratings *IEEE Photonics Technol. Lett.* **26** 829–32
[12] Vasil'eva V V, Vinokurov D A, Zolotarev V V, Leshko A Y, Petrunov A N, Pikhtin N A, Rastegaeva M G, Sokolova Z N, Shashkin I S and Tarasov I S 2012 High-order diffraction gratings for high-power semiconductor lasers *Semiconductors* **46** 241–6
[13] Zolotarev V V, Leshko A Y, Pikhtin N A, Slipchenko S O, Sokolova Z N, Lubyanskiy Y V, Voronkova N V and Tarasov I Y S 2015 Integrated high-order surface diffraction gratings for diode lasers *Quantum Electron.* **45** 1091
[14] Zolotarev V V, Leshko A Y, Shamakhov V V, Nikolaev D N, Golovin V S, Slipchenko S O and Pikhtin N A 2019 Continuous wave and pulse (2–100 ns) high power AlGaAs/GaAs laser diodes (1050 nm) based on high and low reflective 13th order DBR *Semicond. Sci. Technol.* **35** 015009
[15] Seibert C S, Yuan W, Hall D C, Luo X, Moretti T and Sugg A R 2010 High-index-contrast single output teardrop laser fabricated via oxygen-enhanced non-selective oxidation *Conf. on Lasers and Electro-Optics* (Optica Publishing Group) p JTuD106
[16] Wangqing Y, Seibert C S and Hall D C 2011 Single-facet teardrop laser with matched-bends design *IEEE J. Sel. Top. Quantum Electron.* **17** 1662–9
[17] Kleijn E, De Vries T, Ambrosius H, Smit M K and Leijtens X J M 2010 MMI reflectors with free selection of reflection to transmission ratio *Proc. 15th Annual Symp. of the IEEE Photonics Benelux Chapter* (*Delft, The Netherlands*, *18–19 November 2010*) p 19
[18] Xu L, Leijtens X J M, Docter B, Vries T, Smalbrugge E, Karouta F and Smit M K 2009 MMI-reflector: a

J. Phys. D: Appl. Phys. **56** (2023) 384001

F T Albeladi *et al*

novel on-chip reflector for photonic integrated circuits *2009 35th European Conf. on Optical Communication* pp 1–2

[19] Soldano L B and Pennings E C M 1995 Optical multi-mode interference devices based on self-imaging: principles and applications *J. Lightwave Technol.* **13** 615–27

[20] Spiekman L H, Oei Y S, Metaal E G, Groen F H, Moerman I, Smit M K and Verbeek B H 1994 Extremely small fabrication tolerant InP-based power-splitting and combining structures by deep etching *Proc. European Con$ Opt. Commun. (ECOC)* (*Firenze, Italy*, *September 1994*) p We.C.2.3

[21] Zhao J, Kleijn E, Williams P J, Smit M K and Leijtens X J M On-chip laser with multimode interference reflectors

realized in a generic integration platform *2011-23rd Int. Conf. on Indium Phosphide and Related Materials* (IEEE) pp 1–4

[22] Kleijn E, Smit M K and Leijtens X J M 2013 Multimode interference reflectors: a new class of components for photonic integrated circuits *J. Lightwave Technol.* **31** 3055–63

[23] Smowton P M, Sandall I C, Liu H Y and Hopkinson M 2007 Gain in p-doped quantum dot lasers *J. Appl. Phys.* **101** 013107

[24] Smowton P M, Sandall I C, Mowbray D J, Hui Yun L and Hopkinson M 2007 Temperature-dependent gain and threshold in p-doped quantum dot lasers *IEEE J. Sel. Top. Quantum Electron.* **13** 1261–6